

This discussion paper is/has been under review for the journal *Atmospheric Chemistry and Physics (ACP)*. Please refer to the corresponding final paper in *ACP* if available.

**Eddy covariance  
methane  
measurements**

C. J. P. P. Smeets et al.

# Eddy covariance methane measurements at a Ponderosa pine plantation in California

C. J. P. P. Smeets<sup>1</sup>, R. Holzinger<sup>1</sup>, I. Vigano<sup>1</sup>, A. H. Goldstein<sup>2</sup>, and T. Röckmann<sup>1</sup>

<sup>1</sup>Institute for Marine and Atmospheric research Utrecht, Princetonplein 5, 3584 CC, Utrecht, The Netherlands

<sup>2</sup>University of California, Berkeley, Department of Environmental Science, Policy and Management, USA

Received: 15 December 2008 – Accepted: 26 January 2009 – Published: 26 February 2009

Correspondence to: C. J. P. P. Smeets (c.j.p.p.smeets@uu.nl)

Published by Copernicus Publications on behalf of the European Geosciences Union.

Title Page

Abstract

Introduction

Conclusions

References

Tables

Figures

◀

▶

◀

▶

Back

Close

Full Screen / Esc

Printer-friendly Version

Interactive Discussion



## Abstract

Long term methane flux measurements have been mostly performed with plant or soil enclosure techniques on specific components of an ecosystem. New fast response methane analyzers make it possible to use the eddy covariance (EC) technique instead. The EC technique is advantageous because it allows continuous flux measurements integrating over a larger and more representative area including the complete ecosystem, and allows fluxes to be observed as environmental conditions change naturally without disturbance. We deployed the closed-path Fast Methane Analyser (FMA) from Los Gatos Research Ltd and demonstrate its performance for EC measurements at a Ponderosa pine plantation at the Blodgett Forest site in central California. CH<sub>4</sub> concentrations measured at 10 Hz showed a relatively high noise level that was caused by a software related problem. Nevertheless, in the frequency range important for turbulent exchange, the cospectra of CH<sub>4</sub> compare very well with all other scalar cospectra confirming the quality of the FMA measurements are good for the EC technique. The low-pass filtering characteristics of our closed-path system and the use of the Webb-Pearman-Leuning (WPL) corrections for a combination of open and closed-path sensors are discussed using a large ensemble of cospectra. The diurnal variation of the methane concentration was up to 60 ppbv with an average of 1843 ppbv. Concentrations increased from morning to late afternoon as upslope flow from the valley below carried polluted air to the site, and then decreased through the night as downslope flow carried cleaner air from aloft. The fluxes were consistently directed downward with a well defined diurnal pattern, averaging  $-35 \pm 40 \text{ ng m}^{-2} \text{ s}^{-1}$  during the daytime. The detection limit of the system was estimated at  $22 \text{ ng m}^{-2} \text{ s}^{-1}$ . The average CH<sub>4</sub> deposition during the daytime was higher than the average value for warm temperate forests in a recent global inventory and the results from a process-based model study.

ACPD

9, 5201–5229, 2009

### Eddy covariance methane measurements

C. J. P. P. Smeets et al.

Title Page

Abstract

Introduction

Conclusions

References

Tables

Figures

⏪

⏩

◀

▶

Back

Close

Full Screen / Esc

Printer-friendly Version

Interactive Discussion



## 1 Introduction

Methane (CH<sub>4</sub>) is the predominant hydrocarbon in the Earth's atmosphere. Although its abundance is far less than that of carbon dioxide (CO<sub>2</sub>), its greenhouse warming potential is 21 times higher per molecule on a 100 year time horizon resulting in a 18% contribution to the total anthropogenic radiative forcing from greenhouse gases (IPCC, 2007). Current estimates of some of the individual source and sink magnitudes in the CH<sub>4</sub> global budget have significant uncertainties that need to be resolved. In particular, there is scientific controversy over both the magnitude and direction of the CH<sub>4</sub> flux between forests and the atmosphere, and data to solve this controversy are scarce.

The mayor uncertainty is for tropical forests which comprise a large part of all forested land and are the dominant components of the terrestrial biosphere-atmosphere exchange of trace gases. Recent publications by Frankenberg et al. (2005); Braga do Carmo et al. (2006); Miller et al. (2007) from satellite, airplane and ground measurements, respectively, all indicate higher methane emissions from tropical rainforests in the Amazone region than expected from process-based model estimates. Apart from wetlands, other unknown sources of methane emissions are thought to be important contributors as well. Recent laboratory results e.g. from Keppler et al. (2005), Keppler et al. (2008) and Vigano et al. (2008) suggest that plants may be direct emitters of CH<sub>4</sub>.

Long term methane flux measurements in forested areas have been mostly performed using dynamic enclosure (or chamber) techniques for individual ecosystem components such as plants or soils (e.g., Singh et al., 1997; Kiese et al., 2003; Verchot et al., 2000; Kutzbach et al., 2007). While these techniques can be simple and relatively inexpensive to operate, they are not continuous and are prone to a variety of potential errors (e.g., Kutzbach et al., 2007). Moreover, enclosure techniques observe fluxes for very small surface areas which are not necessarily representative of the whole ecosystem and can be easily disturbed by the measurement enclosure itself. For example, Simpson et al. (1999) and Sinha et al. (2007) measured methane fluxes in boreal forests with chambers and exclusively detected net uptake of CH<sub>4</sub>, while fluxes

### Eddy covariance methane measurements

C. J. P. P. Smeets et al.

Title Page

Abstract

Introduction

Conclusions

References

Tables

Figures

◀

▶

◀

▶

Back

Close

Full Screen / Esc

Printer-friendly Version

Interactive Discussion



measured from micrometeorological towers showed the importance of spatial source and sink heterogeneity and demonstrated that the forest as a whole as a net source.

The eddy covariance (EC) technique is ideally suited for continuous flux measurements integrating over a larger and more representative area including the complete ecosystem, allowing fluxes to be observed as environmental conditions change naturally without disturbance. Recently, methane analyzers have become available that have a fast enough response time to perform EC flux measurements of methane (e.g. Hendriks et al., 2008; Kroon et al., 2007; Wille et al., 2008). We tested the DLT-100 Fast Methane Analyser (FMA) from Los Gatos Research (LGR) Ltd incorporated for EC flux measurements over a Ponderosa pine plantation at the Blodgett Forest site on the western slope of the Sierra Nevada Mountains in California. In the near future we plan to test the recent hypothesis of higher methane emissions in the Amazon basin. The FMA is a closed path methane analyzer with a response rate up to 20 Hz and is comparatively easy to use, relatively inexpensive, and stable over longer periods (Hendriks et al., 2008). We present a thorough evaluation of the EC data quality and processing with an emphasis on the frequency-dependent response functions. Special attention is given to the complications that arise when applying Webb-Pearman-Leuning (WPL) corrections (Webb et al., 1980) to an EC-system that combines open and closed-path measurements. Furthermore, the diurnal variations of CH<sub>4</sub> concentrations and fluxes are discussed and compared to findings from a recent global inventory (Dutaur and Verchot, 2007) and process-based model calculations (Ridgwell et al., 1999).

## 2 Experimental set-up

### 2.1 Field area description

Observations were made from 11 to 19 August 2007, above a Ponderosa pine plantation owned by Sierra Pacific Industries, adjacent to the University of California at Berkeley's Blodgett Forest Research Station. The site is situated on the western slope

## Eddy covariance methane measurements

C. J. P. P. Smeets et al.

Title Page

Abstract

Introduction

Conclusions

References

Tables

Figures

⏪

⏩

◀

▶

Back

Close

Full Screen / Esc

Printer-friendly Version

Interactive Discussion



of the Sierra Nevada mountains in California (38.90° N, 120.63° W, and 1315 m elevation), 75 km downwind (northeast) of Sacramento and receives anthropogenically impacted air masses rising from the valley below during the day. The site was planted with *Pinus ponderosa* L. in 1990, interspersed with a few individuals of Douglas fir, white fir, California black oak, and incense cedar. Average canopy height in July 2007 was about 8 m, and the leaf area index was estimated as  $3.2 \text{ m}^2 \text{ m}^{-2}$ . The understory was composed primarily of manzanita (*Arctostaphylos* spp.) and whitethorn (*Ceanothus cordulatus*) shrubs. A detailed description of the site is provided by Goldstein et al. (2000) and Misson et al. (2005).

The EC measurements were carried out at the top of a 13.5 m high scaffolding tower. The instrumentation consisted of a Campbell CSAT3 sonic anemometer, a Campbell FW3 Type E thermocouple, a LI-COR LI7500 open-path hygrometer, and a Fast Methane Analyzer (FMA, Los Gatos Research). Raw data was sampled at 10 Hz using a Campbell CR1000 datalogger and stored on a laptop. The FMA was operated in a closed-path EC set-up that carries the sampled air through a 20 m long PVC tube with a 1 cm inner diameter. The tube inlet was shielded from rain by a funnel that was mounted 0.2 m behind the sonic anemometer and close to the LI7500. Before the air enters the cavity it passes a Swagelok SS-4FW4 internal filter with a  $2 \mu\text{m}$  pore size. The pump is a high flow dry scroll pump XDS-35i from BOC Edwards with a maximum pumping capacity of  $580 \text{ l min}^{-1}$  that is placed behind the FMA. The FMA and dry scroll pump were placed in water resistant and ventilated aluminium boxes. The resistance within the system reduces the pumping speed and from the time lag between the sonic anemometer and the FMA signal we estimated it to be about  $40 \text{ l min}^{-1}$ .

The EC measurements were installed 5.5 m above a medium dense canopy at a height of about  $z=13.5 \text{ m}$ . The presence of the canopy causes the bottom surface only to take up a small fraction of the total shear stress. In other words, the logarithmic velocity profile has its origin at the level where the canopy-averaged surface stress acts, the so-called displacement height  $d$ . This length scale is used as a zero reference level in order to obtain a representative measurement height ( $z-d$ ). Following Wieringa

**Eddy covariance  
methane  
measurements**

C. J. P. P. Smeets et al.

Title Page

Abstract

Introduction

Conclusions

References

Tables

Figures

◀

▶

◀

▶

Back

Close

Full Screen / Esc

Printer-friendly Version

Interactive Discussion



(1993), we assume that  $d$  is proportional to the height of the canopy ( $h$ ), i.e.  $d/h=0.7$ , so that the representative measurement height becomes  $z-d=7.9$  m.

### 3 Data processing

#### 3.1 General corrections

5 To correct for the frequency responses in our EC-system we follow the approach of Moore (1986). The methods and transfer functions applied are fully described in the Appendix.

EC measurements are always subject to imperfect leveling and we force the individual half hourly averages of the sonic anemometer wind speeds perpendicular to the average wind direction and in the vertical to zero, i.e.  $\bar{v}=0$  and  $\bar{w}=0$ .

10 The delay times between the raw data signals from the sonic anemometer and the open and closed path sensors were detected by a trial and error method that maximizes the covariances. The mean time delay for the closed path system was found to be about 2.6 s. This procedure also corrects for the longitudinal (streamwise) separation of sensors while the lateral separation (i.e., perpendicular to the mean wind direction) is corrected separately (see Sect. A1).

The sonic temperature flux is corrected for the contamination from humidity fluxes (Schotanus et al., 1983). The CSAT3 sonic anemometer is corrected internally for the influence of velocity fluctuations.

20 Low-pass filtering of scalar fluctuations inside the sampling tube of a closed-path system can lead to considerable high frequency loss (Lenschow and Raupach, 1991). The theoretical transfer function by Lenschow and Raupach (1991) appears to underestimate the actual tube damping in accord with the findings of Aubinet et al. (2001) and Spank and Bernhofer (2008). We corrected for this by adding an empiric correction factor to their transfer function (Sect. A2).

## Eddy covariance methane measurements

C. J. P. P. Smeets et al.

Title Page

Abstract

Introduction

Conclusions

References

Tables

Figures

◀

▶

◀

▶

Back

Close

Full Screen / Esc

Printer-friendly Version

Interactive Discussion



## 3.2 WPL corrections

Density fluctuations arising from heat and water vapor fluxes affect the measured flux densities of trace gases, such as moisture and CO<sub>2</sub> according to the Webb-Pearman-Leuning (WPL) theory (Webb et al., 1980). The assumptions by WPL (i.e., no net flux of dry air) lead to the prediction of a mean vertical velocity in the presence of heat and/or water vapor fluxes. The vertical flux density  $F_c$  of  $c$ , with density  $\rho_c$ , is given as follows in the WPL formulation

$$F_c = \overline{\rho'_c w'} + \overline{\rho_c w} = \overline{\rho'_c w'} + \overline{\rho_c} \left[ \frac{\mu}{\overline{\rho_d}} \overline{w' \rho'_v} + \frac{(1 + \mu\sigma) \overline{w' T'}}{\overline{T}} \right] \quad (1)$$

with  $w$  the vertical velocity, indices  $v$  and  $d$  indicate the water vapor and the dry air component, respectively,  $T$  is the temperature,  $\mu$  is the ratio of the molecular masses dry air and water vapor ( $m_d/m_v=1.61$ ),  $\sigma$  is the water vapor mixing ratio ( $\overline{\rho_v}/\overline{\rho_d}$ ). Overbars represent time-mean quantities and primes represent deviations from the mean. The first term on the right hand side of Eq. (1) is the measured scalar flux and the second term determines the WPL correction due to the contributions of the water vapor and heat fluxes. We apply WPL-theory by following the specific recommendations for closed path sensors by Ibrom et al. (2007a) summarized below.

The temperature flux in Eq. (1) is set to zero since the damping of temperature fluctuations inside the tube of the closed path system is very effective. This only leaves the dilution term by water vapor fluctuations in Eq. (1). For a closed path FMA this specifically refers to the fluctuations inside the measurement cell where the methane concentrations are measured. Henceforth, when considering the water vapor flux from the open-path LI7500 with the WPL-theory, it should be reduced by the attenuation effects by tube damping and cell volume averaging. Additionally, a significant delay in travel time of water vapor through the tube with respect to other scalars has been found in several experiments (Laubach and Teichmann, 1996; Aubinet et al., 2000; Clement, 2004; Ibrom et al., 2007a,b). The latter quantify the effects in dependence of

Title Page

Abstract

Introduction

Conclusions

References

Tables

Figures

◀

▶

◀

▶

Back

Close

Full Screen / Esc

Printer-friendly Version

Interactive Discussion



the relative humidity. This decoupling of scalars and water vapor desynchronizes the actual dilution of the scalars (i.e.  $\text{CH}_4$ ) by water vapor inside the closed-path FMA (i.e., the WPL effect). Since we currently do not know the effect of scalar decoupling in our system, we estimated these from the results of Ibrom et al. (2007b) (Sect. A5).

### 5 3.3 High frequency noise

The amplitude of typical 30-min variations of methane concentrations during the experiment was only about a factor two or three larger than the noise level. The typical amplitude of signal noise was about  $\pm 5$  ppbv which appeared to be related to the data acquisition system; recently upgraded software reduces the noise level to  $\pm 1$  ppbv. The consequence of a high noise level is a typical slope of +1 at the high frequency end of the power spectrum, which is commonly referred to as white noise (Stull, 1997). The cospectrum is much less influenced since the random noise signal does not correlate with vertical wind speed variations. Such filtering capacity of the covariance function was also demonstrated by Wienhold et al. (1995). Nevertheless, noise still partly modifies the high frequency end of our cospectra. In Fig. 1 we plotted averaged and normalised cospectra from a selection of 87 runs (see Appendix for a list of selection criteria). The cospectra were corrected for sensor line-averaging and/or a lateral separation correction when appropriate.

The cospectra of sensible heat and water vapor ( $C_{wT_s}$  and  $C_{wq}$ ) overlap and compare very well to the (arbitrarily offset) universal Kansas curve for neutral cospectra (Kaimal, 1973). This result is proof for the high quality of our EC measurements. The selected cospectra were obtained under slightly unstable conditions (see Appendix) which explains their increase relative to the universal curve at the low frequency end (distance  $A > B$  in Fig. 1). The cospectrum of  $\text{CH}_4$  also compares very well to the other cospectra, thereby confirming the good quality of the  $\text{CH}_4$  measurements by the FMA. However, for frequencies higher than  $f = 0.3$  Hz (vertical dotted line) the values behave erratic due to the signal noise. The dotted curve demonstrates how  $C_{w\text{CH}_4}$  is expected to vary without the influence of signal noise. This curve was calculated from reducing

## Eddy covariance methane measurements

C. J. P. P. Smeets et al.

Title Page

Abstract

Introduction

Conclusions

References

Tables

Figures

◀

▶

◀

▶

Back

Close

Full Screen / Esc

Printer-friendly Version

Interactive Discussion



$C_{wT_s}$  with the transfer functions for tube damping, lateral sensor separation and cell volume damping (Appendix).

We filter out the random contribution of signal noise by calculating the CH<sub>4</sub> fluxes from all cospectral estimates with  $f < 0.3$  Hz. The contribution to the fluxes above  $f = 0.3$  Hz is estimated from the relative contributions in this frequency range to the sensible heat, water vapor and CO<sub>2</sub> fluxes under the assumption of cospectral similarity of scalars (i.e. this is confirmed in Fig. 1). For the ensemble of 87 cospectra the average contribution was about 7% and varied between 3 and 11%.

### 3.4 Calculation of the methane fluxes

In this Section we summarise the calculation of methane fluxes and quantify the effect of several corrections for the ensemble of 87 runs obtained during the daytime.

After maximizing the covariances via a trial and error method, the cospectra are calculated and all appropriate transfer functions are applied. The influence of instrument noise on the CH<sub>4</sub> fluxes for  $f > 0.3$  Hz is removed following the procedure discussed in the previous Section.

Before the WPL corrections can be applied to the CH<sub>4</sub> fluxes, we need an estimate of the water vapor flux inside the measurement cell. First, the true free atmospheric water vapor cospectra are calculated from the open-path LI7500 data by applying corrections for lateral separation and sensor line averaging. The cospectra of the water vapor flux inside the measurement cell of the FMA are then simulated by decreasing the free atmospheric cospectra with the inverted transfer functions for tube damping and cell volume averaging (the flux is reduced by 1–5%). These reductions are small as a result of the combination of a relatively short and wide tube and a high flow rate compared to other closed path systems. Additionally, we apply a transfer function to correct for the effect of phase shifts (Ibrom et al., 2007b) in the system between scalars and water vapor using the maximum relative humidity found during the daytime (i.e. RH=35%, see Fig. 2). The desynchronisation between the water vapor and CH<sub>4</sub> signal reduces the water vapor fluxes in the WPL correction by 2–11% (Sect. A5), which simultaneously

Title Page

Abstract

Introduction

Conclusions

References

Tables

Figures

◀

▶

◀

▶

Back

Close

Full Screen / Esc

Printer-friendly Version

Interactive Discussion



reduces the WPL effect.

Taking the free atmospheric water vapor fluxes for the calculation of the WPL effect reduces the average downward  $\text{CH}_4$  flux for the ensemble of runs from  $214$  to  $56 \text{ ng m}^{-2} \text{ s}^{-1}$  (a reduction of 74%). Adding the corrections for tube damping/volume averaging and phase effects reduces the water vapor flux, and with that the WPL effect, so that the average  $\text{CH}_4$  flux increases to  $61$  and  $68 \text{ ng m}^{-2} \text{ s}^{-1}$ , respectively (i.e., the WPL reduction decreases to 71 and 68%, respectively). Hence, for our experiment at the Blodgett forest site, the very low values of RH during the experiment result in a relatively small effect from phase shifts (the  $\text{CH}_4$  flux increases about 10%). However this may be different in other environments such as tropical forests where RH has averages of 80% even in the dry season. Using  $\text{RH}=80\%$  reduces the influence of the WPL effect significantly. The desynchronisation of scalars inside the measurement cell reduces the water vapor flux in the WPL correction about 30%, and with that, the average  $\text{CH}_4$  flux increases to  $99 \text{ ng m}^{-2} \text{ s}^{-1}$ . This is a 46% increase compared to the cases with  $\text{RH}=35\%$ . It should be noted that such large sensitivity to WPL corrections is specific for the relatively small  $\text{CH}_4$  fluxes compared to those for water vapor. As an example we note that the total water vapor flux dilution in the WPL corrections for  $\text{CO}_2$  fluxes only causes the flux to decrease 20%. Nonetheless, it is obvious that low-pass filtering due to phase effects is potentially very important and should therefore be quantified properly for any closed-path EC-system to prevent possible serious underestimation of fluxes.

## 4 Results

In Fig. 2 the mixing ratios of  $\text{CH}_4$  and  $\text{CO}$  are plotted together with the meteorological variables temperature, wind speed, relative humidity, net-radiation and wind direction. The timelines of  $\text{CH}_4$  and  $\text{CO}$  closely follow each other which suggests that both gases originate from the same source regions (Central valley/Sacramento region) and that their mixing ratios are mainly controlled by the diurnal flow patterns. The meteorolog-

### Eddy covariance methane measurements

C. J. P. P. Smeets et al.

Title Page

Abstract

Introduction

Conclusions

References

Tables

Figures

◀

▶

◀

▶

Back

Close

Full Screen / Esc

Printer-friendly Version

Interactive Discussion



ical variables show a clear diurnal variation that illustrates the very regular upslope-downslope flow, described in detail by Lamanna and Goldstein (1999) and Dillon et al. (2002). During summer this circulation is very persistent and present for 72% of the time (Carroll and Dixon, 2002).

5 During the daytime, upslope flow from the warm Central valley rises along the Western slope of the Sierra Nevada. After sunset a shallow stable boundary layer develops due to radiative cooling of the surface and a layer of cold air flows downslope. Along with this regular wind pattern, the Sacramento urban plume is transported up into the foothills of the Sierra Nevada during daytime. After sunset, the pollutants are flushed  
10 back towards Central Valley, being replaced by cleaner regional background air from aloft.

Early in the morning, together with the onset of the upslope flow as indicated by the first vertical solid line in Fig. 2 (at 07:30 h), the concentrations of CH<sub>4</sub> and CO increase simultaneously until the flow turns downslope again at sunset (second vertical solid line  
15 at 18:00 h). This diurnal cycle for CH<sub>4</sub> and CO resembles the results from Lamanna and Goldstein (1999) for anthropogenically emitted hydrocarbons.

The identical behaviour for CH<sub>4</sub> and CO demonstrates that CH<sub>4</sub> originates from the anthropogenic sources around the Sacramento area. While CO emissions mainly originate from combustion, the majority of CH<sub>4</sub> emissions in California comes from landfills  
20 (42%) and agricultural livestock (38%) (Franco, 2002). The latter is heavily concentrated in the Central Valley which makes it probably the most important contributor. The CH<sub>4</sub> concentrations vary around the California ambient air background value of about 1835 ppbv (Rigby et al., 2008) with higher values occurring in the pollution plume from the Sacramento area (late afternoon) and lower ones for the regional background  
25 air originating from higher in the Sierra Nevada (just before sunset).

The time series of the various fluxes are plotted in Fig. 3. For CH<sub>4</sub> fluxes (pink bars) we only plotted those runs for which a realistic phase shift was obtained from the maximization of covariances (a time lag between 2.2 and 3.0 s). The size of the pink bars illustrates the effect of a water vapor phase shift in the WPL corrections (i.e. with

---

## Eddy covariance methane measurements

C. J. P. P. Smeets et al.

---

Title Page

Abstract

Introduction

Conclusions

References

Tables

Figures

◀

▶

◀

▶

Back

Close

Full Screen / Esc

Printer-friendly Version

Interactive Discussion



**Eddy covariance  
methane  
measurements**

C. J. P. P. Smeets et al.

[Title Page](#)[Abstract](#)[Introduction](#)[Conclusions](#)[References](#)[Tables](#)[Figures](#)[◀](#)[▶](#)[◀](#)[▶](#)[Back](#)[Close](#)[Full Screen / Esc](#)[Printer-friendly Version](#)[Interactive Discussion](#)

and without phase effect corresponds to the largest and smallest negative values of a bar, respectively). The CH<sub>4</sub> fluxes outside the selection are plotted as blue dots. The sensible heat, latent heat and CO<sub>2</sub> fluxes all show a clear daily cycle in accord with the fair weather conditions. At night, all fluxes become negligible as the atmosphere becomes stable and turbulence ceases. The methane fluxes show the same diurnal pattern and are consistently directed downward during daytime. The night time CH<sub>4</sub> fluxes have noticeable more scatter than all other fluxes, which relates to the higher uncertainty of the CH<sub>4</sub> measurements.

The daily maximum (downward) CH<sub>4</sub> flux varies around 100 ng m<sup>-2</sup> s<sup>-1</sup> (or 8.6 mg m<sup>-2</sup> day<sup>-1</sup>) and the daily average is about 35 ng m<sup>-2</sup> s<sup>-1</sup> (3.0 mg m<sup>-2</sup> day<sup>-1</sup>). These values were calculated accounting for water vapor phase effects in the WPL corrections assuming RH=35%. The CH<sub>4</sub> fluxes obtained during the Blodgett forest campaign are higher than those from observational and model estimates. A recent global inventory of field measurements conducted in temperate forests estimates an annual average uptake of 1.6 mg m<sup>-2</sup> day<sup>-1</sup> (Dutaur and Verchot, 2007). Ridgwell et al. (1999) used a process-based model to calculate the consumption of atmospheric CH<sub>4</sub> by soils, and their average grid cell value for the experimental region in the month of July is about -1 mg m<sup>2</sup> day<sup>-1</sup>.

Verchot et al. (2000) and Dutaur and Verchot (2007) suggest that soil texture is an important biochemical control of CH<sub>4</sub> oxidation in soils with coarse textured soils consuming CH<sub>4</sub> most efficient. Given the very dry conditions at the Blodgett forest site throughout summer, it is likely that during our measurements the CH<sub>4</sub> uptake by the soil was not limited by oxidation reactions in the soil but through its gas-phase transport capacity, i.e., how well the ground is drained (Verchot et al., 2000). In line with this, the diurnal variation of sub-surface temperatures and humidity were not found to correlate with the measured CH<sub>4</sub> fluxes. Since the soil at the Blodgett forest site is very porous (up to 65% by volume, Goldstein et al., 2000) we therefore expect a high gas diffusivity that is likely to support the observation of relatively high CH<sub>4</sub> fluxes.

Most results from other studies using EC systems to measure CH<sub>4</sub> fluxes were ob-

**Eddy covariance  
methane  
measurements**

C. J. P. P. Smeets et al.

[Title Page](#)[Abstract](#)[Introduction](#)[Conclusions](#)[References](#)[Tables](#)[Figures](#)[⏪](#)[⏩](#)[◀](#)[▶](#)[Back](#)[Close](#)[Full Screen / Esc](#)[Printer-friendly Version](#)[Interactive Discussion](#)

tained under conditions providing much higher fluxes, e.g. an average of  $480 \text{ ng m}^{-2} \text{ s}^{-1}$  over a peat meadow area (Hendriks et al., 2008),  $50$  to  $350 \text{ ng m}^{-2} \text{ s}^{-1}$  over Arctic tundra (Wille et al., 2008), and an average of  $680 \text{ ng m}^{-2} \text{ s}^{-1}$  over peat grassland (Kroon et al., 2007). We analyzed the detection limit for our  $\text{CH}_4$  fluxes following the method described by Wienhold et al. (1995) and also used by Kroon et al. (2007). In short, multiple covariances (or cross covariances) are calculated using a wide range of time lags between e.g.  $w'$  and  $\text{CH}_4'$  (we used a range between  $-50$  and  $+50$  s and calculated the covariance every  $0.1$  s). The standard deviation of the cross covariances far outside the true lag time is used as an estimate for the flux detection limit (i.e., values between  $-50$  to  $-40$  and  $+40$  to  $+50$  s). Since the  $\text{CH}_4$  covariances also include WPL effects we corrected for this using a simple error analysis (Sect. A6). The average probable detection limit for the ensemble of 87 runs is estimated at  $22 \text{ ng m}^{-2} \text{ s}^{-1}$  with a standard deviation of  $12 \text{ ng m}^{-2} \text{ s}^{-1}$ . The uncertainty of fluxes above the detection limit is on average 26%. As a comparison, the uncertainty for all other fluxes obtained with the same method is about 6%, a factor 4 lower. Note, as mentioned before, that the results for  $\text{CH}_4$  are influenced by large instrumental noise resulting from outdated instrument software. Implementation of new software reduces the signal-to-noise ratio of the FMA a factor 5 (I. Vigano, personal communication, 2008) and is expected to lower the detection limit.

## 5 Conclusions

We have shown the feasibility of EC measurements at low  $\text{CH}_4$  flux levels with a Fast Methane Analyser (FMA) during an experiment in a Ponderosa pine plantation at the Blodgett Forest site in California. Even with a relatively high signal to noise ratio due to inferior instrument software, the detection limit of the system was about  $22 \text{ ng m}^{-2} \text{ s}^{-1}$  with an average uncertainty for fluxes above the detection limit of 26%. Upgrading the instrument software reduces the noise by a factor 5, and hence, the resolution and lower detection limit for  $\text{CH}_4$  fluxes are expected to improve significantly.

**Eddy covariance  
methane  
measurements**

C. J. P. P. Smeets et al.

Title Page

Abstract

Introduction

Conclusions

References

Tables

Figures

◀

▶

◀

▶

Back

Close

Full Screen / Esc

Printer-friendly Version

Interactive Discussion

The data treatment procedure is presented in detail. The theoretical transfer function for tube damping by Lenschow and Raupach (1991) was found to underestimate the actual damping in line with findings by Aubinet et al. (2000) and Spank and Bernhofer (2008). The cospectra from the CH<sub>4</sub> fluxes compare very well to those from all other scalars and the universal Kansas curve (Kaimal, 1973), demonstrating the quality of the FMA is useful for EC measurements. Nevertheless, the high signal to noise ratio in the CH<sub>4</sub> signal caused erratic behavior of the cospectral estimates at the high frequency end above  $f=0.3$  Hz. This random flux contribution was removed by calculating the CH<sub>4</sub> fluxes from cospectral estimates below the filter frequency  $f=0.3$  Hz. The contribution to the fluxes above  $f=0.3$  Hz was estimated from the corrected cospectra of temperature, water vapor and CO<sub>2</sub>. The effects of desynchronization of the water vapor and CH<sub>4</sub> signals inside a closed path sensor, quantitatively described by Ibrom et al. (2007b), are shown to be potentially very important for the Webb-Pearman-Leuning (WPL) correction (Webb et al., 1980) applied to the relatively small CH<sub>4</sub> fluxes. The magnitude of the effect strongly depends on the relative humidity and implementation for the California data, with a maximum value of only RH=35% during the daytime, the CH<sub>4</sub> flux increases only about 10%. However, in the hypothetic case of a tropical rainforest ecosystem, where RH is typically 80% during the dry season, the increase would be as high as 60%.

The observations at the Blodgett forest site show that the CH<sub>4</sub> concentrations vary diurnally with the upslope flow from the polluted valley below in the day, and the downslope flow of cleaner air from aloft during the night with an average value of about 1843 ppbv. The CH<sub>4</sub> fluxes were consistently directed downward and followed a clear diurnal pattern. Based on an ensemble of 87 30-min flux measurements the average during the daytime was  $35\pm 40$  ng m<sup>-2</sup> s<sup>-1</sup> and the maximum values varied around 100 ng m<sup>-2</sup> s<sup>-1</sup>. These values are higher than recent estimates from a global inventory of field measurements in temperate forests (Dutaur and Verchot, 2007) and a process-based model study (Ridgwell et al., 1999). The very dry conditions and porous soil texture at the Blodgett Forest site support a high gas diffusivity of the soil resulting in

relatively high CH<sub>4</sub> fluxes.

Current estimates of upward directed CH<sub>4</sub> fluxes over tropical forest ecosystems by Braga do Carmo et al. (2006), Miller et al. (2007) and Sinha et al. (2007) give values of about 20 to 210, 280, and 80 ng m<sup>-2</sup> s<sup>-1</sup>, respectively. The EC system presented here is expected to be well suited for measuring the CH<sub>4</sub> fluxes even at the low end of this range.

## Appendix A

### Frequency response corrections for the EC-system

In Moore (1986) simplified expressions are given that describe the frequency response corrections for EC-systems expressed as frequency-dependent cospectral transfer functions. For example, the correction of the water vapor flux by means of a transfer function is given by

$$\frac{\Delta F}{F} = 1 - \int_0^{\infty} T_{wq}(f) C_{wq}(f) df \bigg/ \int_0^{\infty} C_{wq}(f) df \quad (\text{A1})$$

with  $T_{wq}$  the net system cospectral transfer function associated with sensors of vertical velocity  $w$  and quantity  $q$ ,  $C_{wq}$  is the atmospheric cospectrum of  $w$  and  $q$  at frequency  $f$  (Hz). It is the product of the response functions associated with sensor frequency response, size and separation.

The theoretical transfer functions suggested by Moore (1986) and others often underestimate the actual damping in the system (e.g., Spank and Bernhofer, 2008). In the following, we use an ensemble of 87 cospectra to study several theoretical and empiric sensor response functions. To obtain good quality cospectra for the ensemble we use the following criteria. After rotation of the EC data (i.e., forcing  $\bar{v}$  and  $\bar{w}$  to zero) and in case of a stationary and homogeneous boundary layer in two-dimensional and axially

Title Page

Abstract

Introduction

Conclusions

References

Tables

Figures

◀

▶

◀

▶

Back

Close

Full Screen / Esc

Printer-friendly Version

Interactive Discussion



## Eddy covariance methane measurements

C. J. P. P. Smeets et al.

Title Page

Abstract

Introduction

Conclusions

References

Tables

Figures

◀

▶

◀

▶

Back

Close

Full Screen / Esc

Printer-friendly Version

Interactive Discussion



symmetric flow, the momentum flux perpendicular to the average wind direction,  $\overline{v'w'}$ , should now equal zero. In practice this is seldom the case and we therefore limit the ratio of the lateral and longitudinal momentum fluxes to  $\left| \overline{v'w'}/\overline{u'w'} \right| < 0.25$ . The friction velocity  $u_*$  should exceed  $0.1 \text{ ms}^{-1}$ . To obtain realistic fluxes, the empiric method that maximizes the covariances should converge to values between 2.2 and 3.0 s for CH<sub>4</sub> and between 0 and 0.3 s for CO<sub>2</sub> and H<sub>2</sub>O (i.e., the average delay time for the closed path sensor was 2.6 s). Furthermore, we only allow runs that were obtained during daytime to obtain a selection of sufficiently large fluxes and consistently unstable conditions, i.e.  $-0.5 < (z-d)/L < 0$  with  $z$  the measurement height and  $L = -u_*^3 \theta_v / \text{kg} w \theta_v$  the Monin-Obukhov length with  $g$  the gravitational acceleration,  $\theta_v$  the virtual potential temperature, and  $\overline{w\theta_v}$  the virtual heat or buoyancy flux.

### A1 Lateral sensor separation

The phase shift between signals of the vertical wind speed and scalars from the Licor7500 or FMA are synchronized by a trial and error method that maximizes the covariance. This method also corrects for the longitudinal (streamwise) separation of sensors but not for the de-correlation caused by lateral sensor separation (i.e., perpendicular to the wind direction). The effect of lateral separation  $s$  between two sensors can be represented by the following co-spectral transfer function

$$T_s(n) = e^{-9.9n^{1.5}} \quad (\text{A2})$$

with  $n = fs/u$  the normalised frequency and  $u$  the wind speed. An optimal value for  $s$  is found by comparing Eq. (A2) with the ratio of ensemble averaged and normalised cospectra of the water vapor flux and the sonic temperature flux. Doing so, we inherently assume negligible flux loss for the sonic temperature flux and co-spectral similarity of scalars in the atmosphere (Ibrom et al., 2007b). The difference in sensor-line averaging effects for the sonic and Licor7500 is negligible. A good match is found for

$s=0.17$  m. Since the inlet of the closed path FMA was close to the Licor7500 we use Eq. (A2) and  $s=0.17$  m to correct the lateral separation for both sensors.

## A2 Tube damping

The effects of low-pass filtering in a closed-path EC-system due to mixing effects are wellknown (Lenschow and Raupach, 1991; Leuning and King, 1992) and can lead to considerable high frequency signal loss. For turbulent flow in a circular tube with radius  $a$  it can be shown that the transfer function is

$$G_t^2 = \exp(-160 Re^{-1/8} af^2 X/U^2), \quad (\text{A3})$$

where  $Re$  is the Reynolds number ( $2aU/\nu$ ),  $\nu$  the kinematic viscosity,  $f$  is frequency,  $X$  is the tube length (i.e. 20 m), and  $U$  the flow speed inside the tube ( $8.2 \text{ ms}^{-1}$  during the California experiment). Equation (A3) applies when  $Re_c=2300 < Re < 10^5$ , where  $Re_c$  is the critical Reynolds number at which the flow becomes turbulent.

We use the data from an experiment in Cabauw (The Netherlands) to quantify the tube damping characteristics of our EC-system. We employed the same tube and pumping system but additionally connected a closed path Licor6262 analyser parallel to the FMA. This synchronous set-up allows direct comparison between the  $\text{CH}_4$  results from the FMA and the  $\text{CO}_2$  results from the LI6262. The empiric transfer function for tube damping is calculated from the ratio of averaged and normalised cospectra of the LI6262  $\text{CO}_2$  and the sonic temperature flux (the same procedure as in Sect. A1). The cospectrum of the sonic temperature flux was corrected for sensor line averaging and the cospectra of the  $\text{CO}_2$  and  $\text{CH}_4$  fluxes were corrected for sensor separation, signal processing for Licor6262  $\text{CO}_2$  signal (Sect. A3 below), and volume averaging inside the measurement cells (Sect. A4 below). The remaining difference between the cospectra of temperature and  $\text{CO}_2/\text{CH}_4$  represents the tube damping.

In Fig. 4 we compare the ratio of normalised cospectra with the predictions from Eq. (A3). First of all, the empiric transfer functions from the  $\text{CO}_2$  and  $\text{CH}_4$  cospectra

Title Page

Abstract

Introduction

Conclusions

References

Tables

Figures

◀

▶

◀

▶

Back

Close

Full Screen / Esc

Printer-friendly Version

Interactive Discussion



match very well implicating that tube damping in the CH<sub>4</sub> cospectra is well represented by that in the CO<sub>2</sub> cospectra from the Licor6262. Second, the prediction from Eq. (A3) clearly underestimates the actual tube damping.

Aubinet et al. (2001) also notice a significant underestimation by the theoretical curve and appoint this to the effect of filters in the system which is not taken into account in the predictions. The empiric transfer function from the ratio of cospectra is reproduced by increasing the tube length in Eq. (A3) by a factor of 8 (solid curve in Fig. 4).

### A3 Signal processing in the Licor6262

High frequency attenuation caused by signal processing takes place in the Licor6262 according to Massman (2004). The Licor6262 uses a third-order Bessel filter as an anti-aliasing filter for signal output, the transfer function,  $h_{3B}(\omega)$ , is expressed as

$$h_{3B}(\omega) = 15/(15 - 6\Omega^2) - \mathbf{i}(15\Omega - \Omega^3) \quad (\text{A4})$$

where  $\mathbf{i}$  is the imaginary unit,  $\Omega = 3.0824 \tau_{3B} (\omega/2\pi)$  and  $\tau_{3B}$  is the time constant of the third-order Bessel filter. As in Massman (2004) we use  $\tau_{3B} = 0.2$  s in this study.

### A4 Volume averaging effects of the measurement cell

The spectral transfer function related to volume averaging in a measurement cell is

$$h_{\text{vol}}(\omega) = \frac{\sin^2(\omega\tau_{\text{vol}}/2)}{(\omega\tau_{\text{vol}}/2)^2} \quad (\text{A5})$$

where  $\tau_{\text{vol}}$  is the time constant of the volume averaging effect which is equal to the time needed to fill the chamber and is computed as  $\tau_{\text{vol}} = V_{\text{cham}}/P$  with  $V_{\text{cham}}$  the volume of the measurement cell,  $P$  is the pumping speed in the system ( $P = 38.8$  and  $35.5$  l min<sup>-1</sup> for the experiments in California and Cabauw, respectively). The cell volume for the Licor6262 is  $1.19 \times 10^{-5}$  m<sup>3</sup> and for the FMA it is  $0.55 \times 10^{-3}$  m<sup>3</sup>.

Title Page

Abstract

Introduction

Conclusions

References

Tables

Figures

◀

▶

◀

▶

Back

Close

Full Screen / Esc

Printer-friendly Version

Interactive Discussion



## A5 Decoupling between H<sub>2</sub>O and other scalars in a closed-path system

Many investigations (Laubach and Teichmann, 1996; Aubinet et al., 2000; Ibrom et al., 2007a) find that the lag time of water vapor in closed-path systems is always larger than for CO<sub>2</sub> (or other inert scalars such as CH<sub>4</sub>). Recent publications by Ibrom et al. (2007a) and Ibrom et al. (2007b) specifically address this decoupling of scalars in the tubing system of a closed-path EC system and quantify its effects in terms of a transfer function that depends on the relative humidity of the air sample. The amplitude attenuation and decoupling of scalars and water vapor desynchronize the actual dilution of the scalar by water vapor inside the closed-path system (i.e., the WPL effect). This desynchronisation of the water vapor signal can be simulated the low pass filtering with a first-order recursive filter (Ibrom et al., 2007b)

$$H(f) = \frac{1}{1 + (f/f_c)^2} \quad (\text{A6})$$

where  $f_c$  is the cut-off frequency (the frequency at which the filter reduces the power spectral estimates by a factor 2). Ibrom et al. (2007b) present an exponential function that predicts the increase of  $f_c$  as a function of relative humidity for their EC-system. Moreover, they also demonstrate that the same relation can be used to other EC-systems with very different tube dimensions (i.e., radius and length).

Since we have not yet quantified the effect of phase shifts for our system we use the results from Ibrom et al. (2007b) to simulate the low-pass filtering in our EC-system. From the CO<sub>2</sub> measurements performed in Cabauw we estimated that the cut-off frequency for tube damping is  $f_c=1.042$  Hz. We estimate from Fig. 2 that the maximum value for RH during the daytime is only about 35%, which increases  $f_c$  by a factor of 4 according to Ibrom et al. (2007b). As an alternative to this low humidity case we also estimated the effects for a tropical rainforest ecosystems where RH can be as high as 80% on average during the dry season leading to an increase of  $f_c$  by a factor of 20. The low pass filtering effects of the phase shift differs substantially for both cases

Title Page

Abstract

Introduction

Conclusions

References

Tables

Figures

◀

▶

◀

▶

Back

Close

Full Screen / Esc

Printer-friendly Version

Interactive Discussion



and the average CH<sub>4</sub> flux for the ensemble of 87 selected runs with RH=35 and 80% increases from -68 to -99 ng m<sup>-2</sup> s<sup>-1</sup> (+45%), respectively. Note that with increasing low pass filtering due to phase effects, the WPL effect decreases and the resulting CH<sub>4</sub> fluxes become larger.

## 5 A6 Probable detection limit of the CH<sub>4</sub> fluxes

The correct covariance was calculated by maximizing its value via a trial and error method that repeatedly calculates covariances for a range of lag times between the signals. The standard deviation in the tail of the distribution of different covariances as a function of lag time (the so-called cross covariance function) corresponds to the  
 10 detection limit (Wienhold et al., 1995; Kroon et al., 2007). In order to obtain a sufficiently large range of values, we calculated the covariances for lag times ranging between plus and minus 50 s. The standard deviations in the range of lag times from -50 to -40 and +40 to +50 s were used as an estimate for the detection limit.

The calculation of the detection limit for CH<sub>4</sub> fluxes is not straightforward since it includes the influence of water vapor fluxes via the WPL effect. To estimate the detection limit from Eq. (1) we use the general formula for the absolute error  $\Delta X$  (Fritschen and Gay, 1979) which is equivalent to the total differential of the function  $X$  consisting of several independent variables  $y_j$ , each with its own absolute error  $\Delta y_j$

$$\Delta X = \frac{\Delta y_1 \partial X}{\partial y_1} + \frac{\Delta y_2 \partial X}{\partial y_2} + \dots + \frac{\Delta y_n \partial X}{\partial y_n}. \quad (\text{A7})$$

The partial derivatives calculated from Eq. (1) for the CH<sub>4</sub> and water vapor fluxes are

$$\frac{\partial F_c}{\partial \rho'_c w'} = 1 \quad (\text{A8})$$

## Eddy covariance methane measurements

C. J. P. P. Smeets et al.

Title Page

Abstract

Introduction

Conclusions

References

Tables

Figures

◀

▶

◀

▶

Back

Close

Full Screen / Esc

Printer-friendly Version

Interactive Discussion



and

$$\frac{\partial F_c}{\partial \rho'_v w'} = \frac{\mu}{\rho_d}, \quad (\text{A9})$$

respectively. We assume that the errors in the other terms are small and the errors in the measured  $\text{CH}_4$  and water vapor fluxes (the  $\Delta y_i$ 's in Eq. A7) are equal to the detection limit derived from the cross covariance. This method gives a maximum possible error estimate since we combine the individual errors in all variables in the most unfavorable way. A more likely estimate of the total error is obtained when the individual error terms in Eq. (A7) are combined through a least squares approach (Fritschen and Gay, 1979).

The probable detection limit for the selection of 87 runs is  $22 \text{ ng m}^{-2} \text{ s}^{-1}$  with a standard deviation of  $12 \text{ ng m}^{-2} \text{ s}^{-1}$ . This corresponds to a normalised detection limit of about 25%. As a comparison, the normalised detection limit for all other fluxes is about 6%, hence, a factor 4 lower. As noted before, the results for  $\text{CH}_4$  are biased by high instrument noise caused by outdated instrument software. New software improves the signal-to-noise ratio of the FMA a factor 5 and will substantially lower the detection limit.

*Acknowledgements.* We thank Sierra Pacific Industries for the use of their land and the University of California, Berkeley, Center for Forestry, Blodgett Forest Research station for cooperation in facilitating this research. This work was funded by the Dutch NWO, project number 016.071.605.

## References

Aubinet, M., Grell, A., Ibrom, A., Rannik, Ü., Moncrieff, J., and co authors: Estimates of the annual net carbon and water exchange of European forests: the euroflux methodology, *Adv. Ecol. Res.*, 30, 113–175, 2000. 5207, 5214, 5219

## Eddy covariance methane measurements

C. J. P. P. Smeets et al.

Title Page

Abstract

Introduction

Conclusions

References

Tables

Figures

◀

▶

◀

▶

Back

Close

Full Screen / Esc

Printer-friendly Version

Interactive Discussion



- Aubinet, M., Chermanne, B., Vandenhaute, M., Longdoz, B., Yernaux, M., and Laitat, E.: Long term carbon dioxide exchange above a mixed forest in the belgain ardennes, *Agr. Forest Meteorol.*, 108, 293–315, 2001. 5206, 5218
- 5 Braga do Carmo, J., Keller, M., Dezincourt Dias, J., Barbaso de Camargo, P., and Crill, P.: A source of methane from the upland forests in the brazilian amazon, *Geophys. Res. Lett.*, 33, L04809, doi:10.1029/2005GL025436, 2006. 5203, 5215
- Carroll, J. J. and Dixon, A. J.: Regional scale transport over complex terrain, a case study: tracing the sacramento plume in the sierra nevada of california, *Atmos. Environ.*, 36(23), 3745–3758, 2002. 5211
- 10 Clement, R.: Mass and energy exchange of a plantation forest in scotland using micrometeorological methods, Ph.D. thesis, The University of Edinburgh, Scotland, 2004. 5207
- Dillon, M., Lamanna, M., Schade, G., Goldstein, A., and Cohen, R.: Chemical evolution of the sacramento urban plume: Transport and oxidation, *J. Geophys. Res.*, 107(D5), 4045, doi:10.1029/2001JD000969, 2002. 5211
- 15 Dutaur, L. and Verchot, L. V.: A global inventory of the soil  $\text{CH}_4$  sink, *Global Biogeochem. Cy.*, 21, GB4013, doi:10.1029/2006GB002734, 2007. 5204, 5212, 5214
- Franco, G.: Inventory of Californian greenhouse gas emissions and sinks: 1990–1999, Report No. 600-02-001F, California Energy Commission, 2002. 5211
- 20 Frankenberg, C., Meirink, J. F., Van Weels, M., Platt, U., and Wagner, T.: Assessing methane emissions from global space-borne observations, *Science*, 308, 1010–1014, doi:10.1126/science.1106644, 2005. 5203
- Fritschen, L. J. and Gay, L. W.: *Environmental Instrumentation*. Springer-Verlag, New York, USA, 216 pp., 1979. 5220, 5221
- 25 Goldstein, A., Hultman, N., Fracheboud, J., Bauer, M., Panek, J., Xu, M., Qi, Y., Guenther, A., and Baugh, W.: Effects of climate variability on the carbon dioxide, water, and sensible heat fluxes above a ponderosa pine plantation in the sierra nevada (ca), *Agr. Forest Meteorol.*, 101(2–3), 113–129, 2000. 5205, 5212
- Hendriks, D. M. D., Dolman, A. J., van der Molen, M. K., and van Huissteden, J.: A compact and stable eddy covariance set-up for methane measurements using off-axis integrated cavity output spectroscopy, *Atmos. Chem. Phys.*, 8, 431–443, 2008, <http://www.atmos-chem-phys.net/8/431/2008/>. 5204, 5213
- 30 Ibrom, A., Dellwik, E., Ejling Larsen, S., and Pilegaard, K.: On the use of the webb-pearman-leuning theory for closed-path eddy correlation measurements, *Tellus B*, 59, 937–946,

---

**Eddy covariance  
methane  
measurements**C. J. P. P. Smeets et al.

---

Title Page

Abstract

Introduction

Conclusions

References

Tables

Figures

◀

▶

◀

▶

Back

Close

Full Screen / Esc

Printer-friendly Version

Interactive Discussion



**Eddy covariance  
methane  
measurements**

C. J. P. P. Smeets et al.

Title Page

Abstract

Introduction

Conclusions

References

Tables

Figures

◀

▶

◀

▶

Back

Close

Full Screen / Esc

Printer-friendly Version

Interactive Discussion

2007a. 5207, 5219

Ibrom, A., Dellwik, E., Flyvbjerg, H., Jensen, N. O., and Pilegaard, K.: Strong low-pass filtering effects on water vapour flux measurements with closed-path eddy correlation systems, *Agr. Forest Meteorol.*, 147, 140–156, 2007b. 5207, 5208, 5209, 5214, 5216, 5219

5 IPCC: IPCC Fourth Assessment Report, *Climate Change 2007*, Cambridge University Press, Cambridge, UK, 996 pp., 2007. 5203

Kaimal, J. C.: Turbulence spectra, length scales and structure parameters in the stable surface layer, *Bound.-Lay. Meteorol.*, 4, 289–309, 1973. 5208, 5214

10 Keppler, F., Hamilton, J., Braß, M., and Röckmann, T.: Methane emissions from terrestrial plants under aerobic conditions, *Nature*, 439, 187–191, doi:10.1038/nature04420, 2005. 5203

Keppler, T., Hamilton, J., McRoberts, W., Vigano, I., Braß, M., and Röckmann, T.: Methoxyl groups of plant pectin as a precursor of atmospheric methane: evidence from deuterium labelling studies, *New Phytol.*, 178, 808–814, doi:10.1111/j.1469–8373.2008.02411.x, 2008. 15 5203

Kiese, R., Hewett, B., and Graham, A.: Seasonal variability of N<sub>2</sub>O emissions and CH<sub>4</sub> uptake from tropical rainforest soils of Queensland, Australia, *Global Biogeochem. Cy.*, 17(2), 1043, doi:10.1029/2002GB00214, 2003. 5203

20 Kroon, P. S., Hensen, A., Jonker, H. J. J., Zahniser, M. S., van 't Veen, W. H., and Vermeulen, A. T.: Suitability of quantum cascade laser spectroscopy for CH<sub>4</sub> and N<sub>2</sub>O eddy covariance flux measurements, *Biogeosciences*, 4, 715–728, 2007, <http://www.biogeosciences.net/4/715/2007/>. 5204, 5213, 5220

Kutzbach, L., Schneider, J., Sachs, T., Giebels, M., Nykänen, H., Shurpali, N. J., Martikainen, P. J., and Wilmking, M.: CO<sub>2</sub> flux determination by closed-chamber methods can be seriously 25 biased by inappropriate application of linear regression, *Biogeochemistry*, 4, 1005–1025, 2007. 5203

Lamanna, M. and Goldstein, A.: In-situ measurements of C<sub>2</sub>–C<sub>10</sub> VOCs above a Sierra Nevada ponderosa pine plantation, *J. Geophys. Res.*, 104(D17), 21247–21262, 1999. 5211

30 Laubach, J. and Teichmann, U.: Measuring energy budget components by eddy correlation: Data corrections and application over low vegetation, *Beitr. Phys. Atmos.*, 69(2), 307–320, 1996. 5207, 5219

Lenschow, D. H. and Raupach, M. R.: The attenuation of fluctuations in scalar concentrations through sampling tubes, *J. Geophys. Res.*, 96, 15259–15268, 1991. 5206, 5214, 5217

**Eddy covariance  
methane  
measurements**

C. J. P. P. Smeets et al.

Title Page

Abstract

Introduction

Conclusions

References

Tables

Figures

◀

▶

◀

▶

Back

Close

Full Screen / Esc

Printer-friendly Version

Interactive Discussion

- Leuning, R. and King, K. M.: Comparison of eddy-covariance measurements of CO<sub>2</sub> fluxes by open- and closed-path CO<sub>2</sub> analysers, *Bound.-Lay. Meteorol.*, 59, 297–311, 1992. 5217
- Massman, W. J.: Concerning the measurement of atmospheric trace gas fluxes with open- and closed-path eddy covariance systems: the wpl terms and spectral attenuation, in: *Handbook of micrometeorology*, edited by: Lee, X., Massman, W. J., and Law, B., Kluwer Academic Publishers, Dordrecht, The Netherlands, 133–160, 2004. 5218
- Miller, J. B., Gatti, L. V., D'Amelio, M. T. S., Crotwell, A. M., Dlugokencky, E. J., Bakwin, P., Artaxo, P. P. and Tans, P.: Airborne measurements indicate large methane emissions from the eastern amazon basin, *Geophys. Res. Lett.*, 34, L10809, doi:10.1029/2006GL029213, 2007. 5203, 5215
- Misson, L., Tang, J., Xu, M., McKay, M., and Goldstein, A.: Influences of recovery from clear-cut, climate variability, and thinning on the carbon balance of a young ponderosa pine plantation, *Agr. Forest Meteorol.*, 130, 207–222, 2005. 5205
- Moore, C. J.: Frequency response corrections for eddy correlation systems, *Bound.-Lay. Meteorol.*, 37, 17–35, 1986. 5206, 5215
- Rigby, M., Prinn, R. G., Fraser, P. J., et al.: Renewed growth of atmospheric methane, *Geophys. Res. Lett.*, 35, L22805, doi:10.1029/2008GL036037, 2008. 5211
- Ridgwell, J. R., Marshall, S. J., and Gregson, K.: Consumption of atmospheric methane by soils: a process-based model, *Global Biogeochem. Cy.*, 13(1), 59–70, 1999. 5204, 5212, 5214
- Schotanus, P., Nieuwstadt, F. T. M., and De Bruin, H. A. R.: Temperature measurement with a sonic anemometer and its application to heat and moisture fluxes, *Bound.-Lay. Meteorol.*, 26, 81–93, 1983. 5206
- Simpson, I. J., Edwards, G. C., and Thurtell, G. W.: Variations in methane and nitrous oxide mixing ratios at the southern boundary of a canadian boreal forest, *Atmos. Environ.*, 33, 1141–1150, 1999. 5203
- Singh, J. S., Singh, S., Raghubanshi, A. S., Singh, S., Kashyap, A. K., and Reddy, V. S.: Effects of soil nitrogen, carbon and moisture on methane uptake by dry tropical forest soils, *Plant Soil* 196, 115–121, 1997. 5203
- Sinha, V., Williams, J., Crutzen, P. J., and Lelieveld, J.: Methane emissions from boreal and tropical forest ecosystems derived from in-situ measurements, *Atmos. Chem. Phys. Discuss.*, 7, 14011–14039, 2007, <http://www.atmos-chem-phys-discuss.net/7/14011/2007/>. 5203, 5215



- Spank, U. and Bernhofer, C.: Another simple method of spectral correction to obtain robust eddy-covariance results, *Bound.-Lay. Meteorol.*, 128, 403–422, 2008. 5206, 5214, 5215
- Stull, R.: An introduction to boundary layer meteorology, D. Reidel Publ. Comp., Dordrecht, The Netherlands, 670 pp., 1997. 5208
- 5 Verchot, L. V., Davidson, E. A., Henrique Cattânio, J., and Ackerman, I. L.: Land-use change and biogeochemical controls of methane fluxes in soils of eastern amazonia, *Ecosystems*, 3, 41–56, 2000. 5203, 5212
- Vigano, I., van Weelden, H., Holzinger, R., Keppler, F., McLeod, A., and Röckmann, T.: Effect of UV radiation and temperature on the emission of methane from plant biomass and structural components, *Biogeosciences*, 5, 937–947, 2008,  
10 <http://www.biogeosciences.net/5/937/2008/>. 5203
- Webb, E. K., Pearman, G. I., and Leuning, R.: Correction of the flux measurements for density effects due to heat and water vapour transfer, *Q. J. Roy. Meteorol. Soc.*, 106, 85–100, 1980. 5204, 5207, 5214
- 15 Wienhold, F. G., Welling, M., and Harris, G. W.: Micrometeorological measurements and source region analysis of nitrous oxide fluxes from an agricultural soil, *Atmos. Environ.*, 29(17), 2219–2227, 1995. 5208, 5213, 5220
- Wieringa, J.: Representative roughness parameters for homogeneous terrain, *Bound.-Lay. Meteorol.*, 63, 323–363, 1993. 5205
- 20 Wille, C., Kutzbach, L., Sachs, T., Wagner, D., and Pfeiffer, E.: Methane emission from siberian arctic polygonal tundra: eddy covariance measurements and modeling, *Glob. Change Biol.*, 14, 1395–1408, 2008. 5204, 5213

---

**Eddy covariance  
methane  
measurements**C. J. P. P. Smeets et al.

---

[Title Page](#)[Abstract](#)[Introduction](#)[Conclusions](#)[References](#)[Tables](#)[Figures](#)[I◀](#)[▶I](#)[◀](#)[▶](#)[Back](#)[Close](#)[Full Screen / Esc](#)[Printer-friendly Version](#)[Interactive Discussion](#)

## Eddy covariance methane measurements

C. J. P. P. Smeets et al.

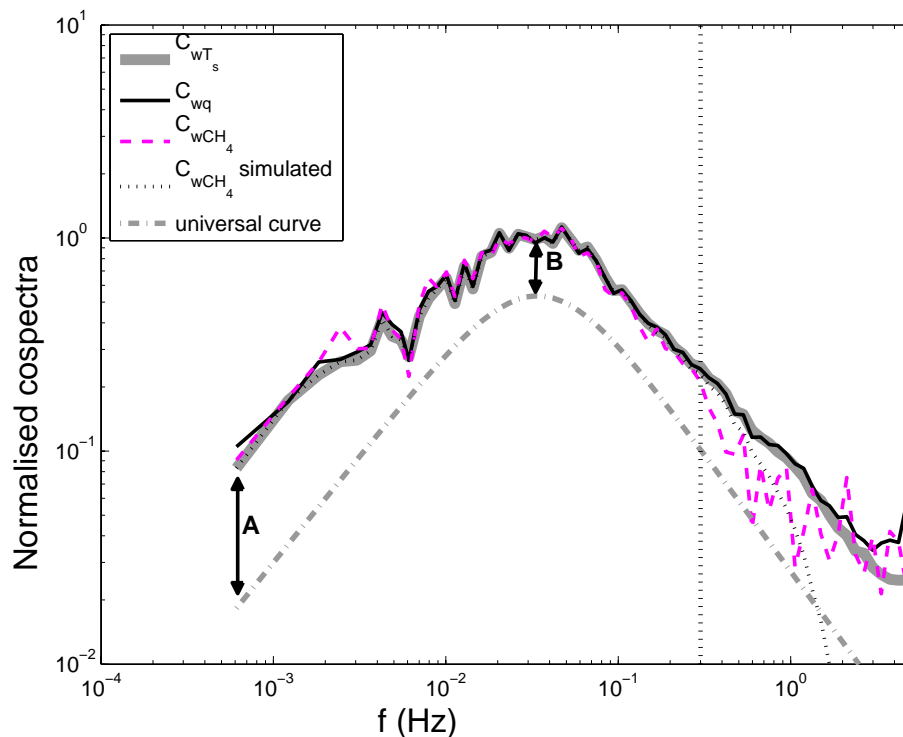


**Fig. 1.** Normalised and averaged cospectra for the sonic temperature flux ( $C_{wT_s}$ ), water vapor flux ( $C_{wq}$ ) and methane flux ( $C_{wCH_4}$ ) as a function of  $f$  (Hz). The dotted curve ( $C_{wCH_4}$  simulated) represents the expected shape of  $C_{wCH_4}$  without the influence of signal noise. The dashed curve is the arbitrarily offset universal cospectrum from Kaimal (1973) for neutral atmospheric stability, arrows **(A)** and **(B)** indicate different deviations from the measured cospectra and the dotted line marks the high frequency region where signal noise contributes to  $C_{wCH_4}$ .

Title Page

Abstract

Introduction

Conclusions

References

Tables

Figures

◀

▶

◀

▶

Back

Close

Full Screen / Esc

Printer-friendly Version

Interactive Discussion



Eddy covariance  
methane  
measurements

C. J. P. P. Smeets et al.

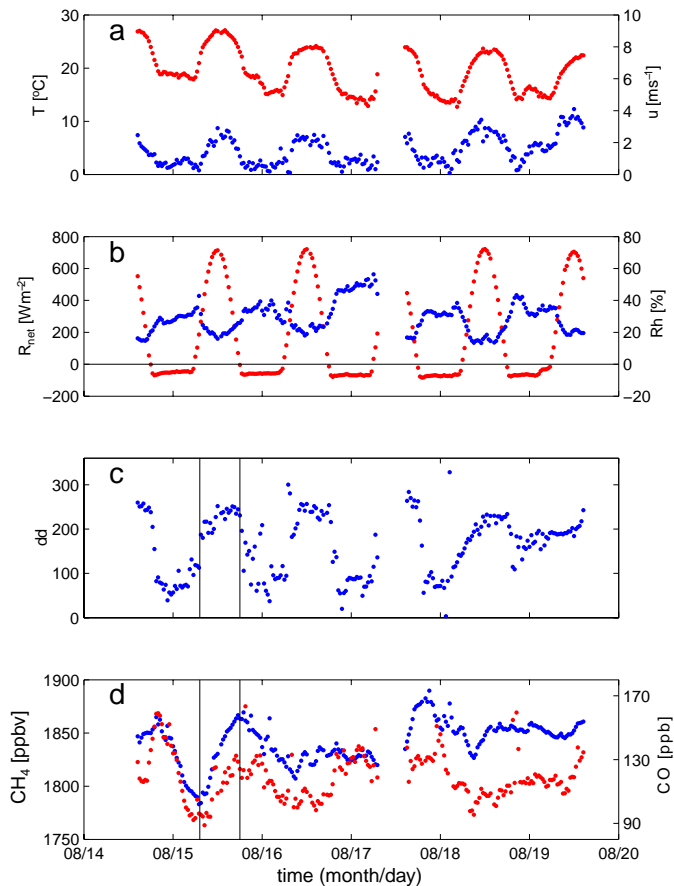


**Fig. 2.** Time series of **(a)** temperature ( $T$ , red) and wind speed ( $u$ , blue), **(b)** net-radiation ( $R_{\text{net}}$ , red) and relative humidity (RH, blue), **(c)** wind direction ( $dd$ ), and **(d)**  $\text{CH}_4$  (blue) and  $\text{CO}$  (red) concentrations as a function of time. The vertical lines in plot (c) and (d) mark the start and reversal of the upslope flow.

Title Page

Abstract

Introduction

Conclusions

References

Tables

Figures

◀

▶

◀

▶

Back

Close

Full Screen / Esc

Printer-friendly Version

Interactive Discussion



Eddy covariance  
methane  
measurements

C. J. P. P. Smeets et al.

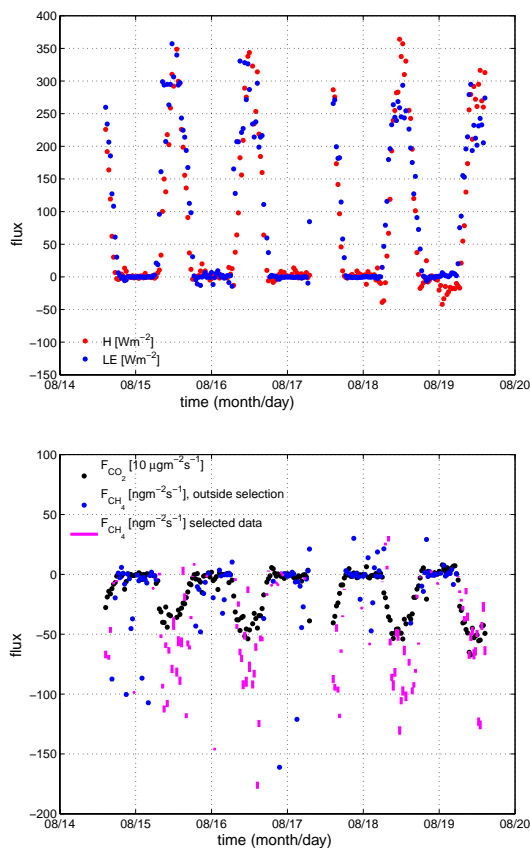


**Fig. 3.** Time series of sensible and latent heat fluxes (upper panel) and  $\text{CO}_2$  and  $\text{CH}_4$  fluxes (lower panel) as a function of time (day of year). The vertical size of the bars for  $\text{CH}_4$  fluxes represent the results with (bottom end of bar) and without (top end of bar) accounting for phase effects in the WPL corrections (see text).

[Title Page](#)[Abstract](#)[Introduction](#)[Conclusions](#)[References](#)[Tables](#)[Figures](#)[◀](#)[▶](#)[◀](#)[▶](#)[Back](#)[Close](#)[Full Screen / Esc](#)[Printer-friendly Version](#)[Interactive Discussion](#)

Eddy covariance  
methane  
measurements

C. J. P. P. Smeets et al.

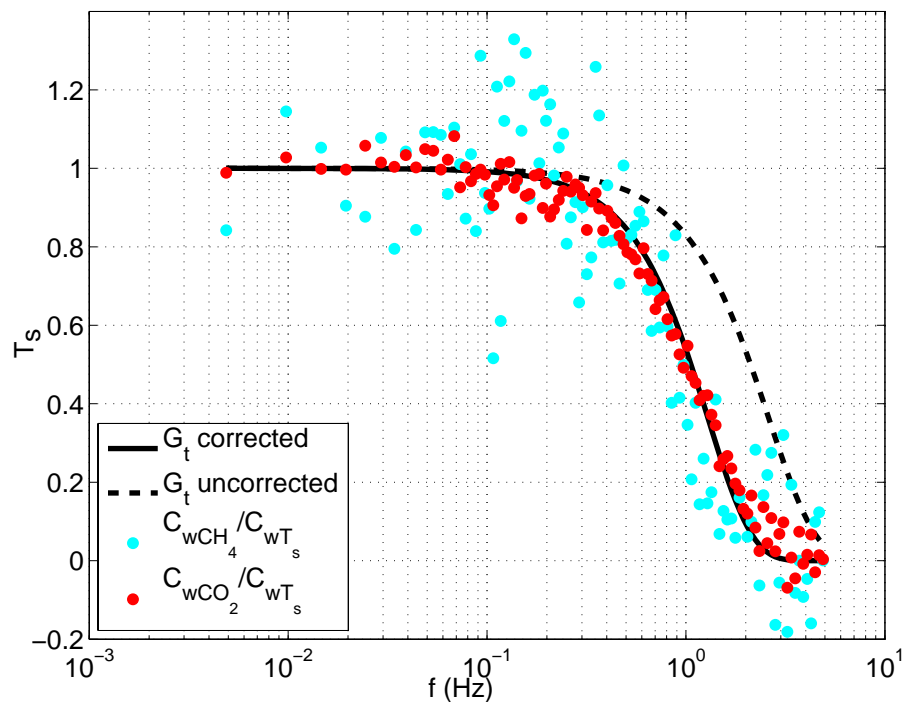


**Fig. 4.** Transfer functions  $T(f)$  for tube damping in the  $\text{CO}_2$  (red dots) and the  $\text{CH}_4$  flux data (blue dots) together with the uncorrected (dashed line) and corrected (solid line) predictions from Eq. (A3) as a function of  $f$  (Hz).

[Title Page](#)[Abstract](#)[Introduction](#)[Conclusions](#)[References](#)[Tables](#)[Figures](#)[◀](#)[▶](#)[◀](#)[▶](#)[Back](#)[Close](#)[Full Screen / Esc](#)[Printer-friendly Version](#)[Interactive Discussion](#)